

# The movement of decanol droplets on surfaces with a chemically patterned energy gradient

I.B. Slootheer & M.H. Markink

Supervisors: Dr. E.S. Kooij and Msc. H.P. Jansen

July 14, 2012

# Abstract

In this report, droplet movement due to a gradient in surface energy is studied. The droplet is a  $2\mu\text{l}$  1-decanol droplet. The gradient is created by forming an array of different chemically striped patterns with alternating hydrophobic and hydrophilic stripes, allowing for reproducible gradients. The hydrophobic stripes are self-assembled monolayers made of hydrophobic fluorinated molecules, while the hydrophilic stripes are the bare  $\text{SiO}_2$  surface of the wafer. The ratio  $\alpha$ , defined as the width of the hydrophobic stripes divided by the width of the hydrophilic stripes, is a key parameter that influences the dynamics of the droplet moving on a surface with a surface energy gradient. Another key parameter for the droplet movement is the absolute width of the hydrophobic and hydrophilic stripes. The movement of the droplet is influenced by the patterned surface underneath the droplet. The droplet tends to move more easily over patterns with wide  $\text{SiO}_2$  stripes. The length of the individual patterns influences the droplet motion as well.

# Contents

<b>Abstract</b>	<b>i</b>
<b>Introduction</b>	<b>1</b>
<b>1 Theory</b>	<b>2</b>
1.1 Contact angle . . . . .	2
1.2 Hydrophobic vs. hydrophilic . . . . .	3
1.3 Advancing and receding edge . . . . .	3
1.4 Energy gradients . . . . .	4
1.5 Forces . . . . .	5
<b>2 Experimental aspects</b>	<b>6</b>
2.1 Pattern creation . . . . .	6
2.2 Individual patterns . . . . .	6
2.3 The dimensionless parameter $\alpha$ . . . . .	7
2.4 Different rows . . . . .	8
2.5 Multiple wafers . . . . .	8
2.6 Droplet deposition and droplet composition . . . . .	9
2.7 Data recording . . . . .	10
<b>3 Analysis</b>	<b>11</b>
3.1 Input . . . . .	11
3.2 Matlab script . . . . .	11
3.3 Positions and velocities . . . . .	12
3.4 Program shortcomings . . . . .	12
3.5 Error bars . . . . .	12
<b>4 Results and discussion</b>	<b>13</b>
4.1 Regimes . . . . .	14
4.2 B row . . . . .	16
4.3 C row . . . . .	16
4.4 D row . . . . .	19
4.5 E row . . . . .	19
4.6 F row . . . . .	22
4.7 G row . . . . .	24
<b>5 Conclusion</b>	<b>26</b>

**Bibliography**

**28**

**Appendix A**

**29**

# Introduction

Modern society relies more and more on complex technology. A major part of the society of the 21st century is the digital world of computers and Internet. Printers are very important for modern-day society because they allow digital information to be transferred into analog information. Ink-jet printers are a very popular kind of printers, using small droplets of ink that are being ejected from nozzles. One of the downsides of these printers is that the nozzles can become clogged.

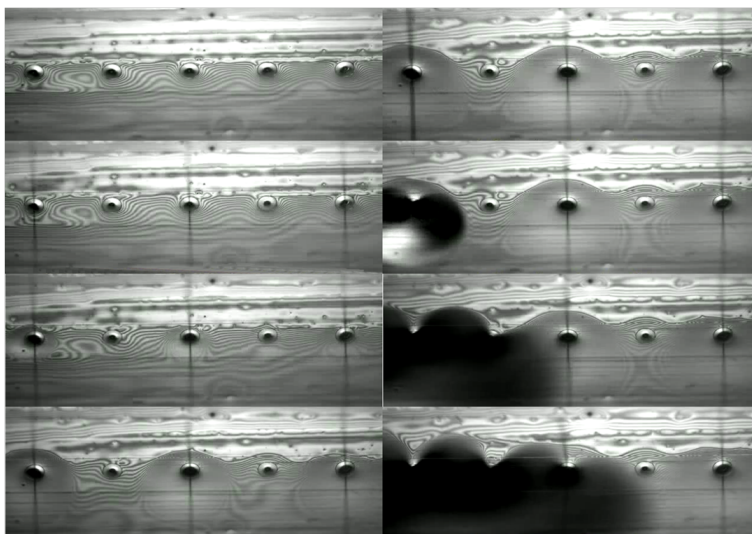


Figure 1: Image of a nozzle of an Ink-jet printer. The nozzle slowly becomes clogged[1]. The chronological order of the images is from the left top to the bottom, followed by the images from the right top to the bottom.

This can be seen in the above figure, Figure 1. This figure shows that as a function of time, the nozzles slowly become clogged because of the ink droplets that do not flow away completely. This leads to a decrease in printing quality and eventually printing will not be possible anymore. The printer needs to be cleaned before printing can proceed. From the industry's point of view, it would be good if a new type of printer, that would not have this problem, will be designed. One way of prohibiting the nozzles to become blocked is to make sure the droplets move away from the nozzle. When a droplet is deposited on a surface with a surface energy gradient, the droplet will start moving to the part with the higher surface energy. In this report, the movement of decanol droplets on surfaces with a chemically engineered surface energy gradient will be studied.

# Chapter 1

## Theory

When a droplet is deposited on a chemically patterned surface, there will be an interaction between the droplet and the surface. This interaction is due to several physical phenomena, which will be discussed in this chapter.

### 1.1 Contact angle

A droplet that comes into contact with a surface will spread to minimize its free energy. The way the droplet spreads depends on both the droplet and the surface. An important parameter of this process is the contact angle, the angle that the droplet makes with the surface. This angle defines the wettability, the strength of the interaction between the liquid and the surface. For an ideal situation, the contact angle can be calculated with Young's equation.

$$\cos(\theta_Y) = \frac{\gamma_{GS} - \gamma_{SL}}{\gamma_{LG}} \quad (1.1)$$

The formula defines the equilibrium between three different kinds of tension: liquid-gas ( $\gamma_{LG}$ ), gas-surface ( $\gamma_{GS}$ ) and liquid-surface ( $\gamma_{SL}$ ), where  $\theta_Y$  is the contact angle[8]. The above equation only holds for ideally smooth surfaces. However, each surface has some degree of roughness, for instance, due to defects. Because of this roughness there is a difference between the apparent contact angle (APCA) and the actual contact angle (ACCA). This difference can best be seen by looking at Figure 1.1.

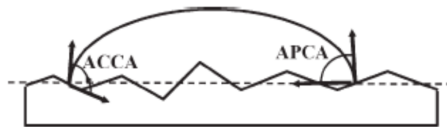


Figure 1.1: Sketch presenting differences in the actual contact angle (ACCA) and the apparent contact angle (APCA)[8].

The actual contact angle is determined locally and therefore takes the roughness into account. The apparent contact angle on the other hand, is defined as the angle between

the tangent to the liquid-gas interface and the straight line that represents the surface. The APCA and ACCA are related through the following formula, the Wenzel formula:

$$\cos(\theta_W) = r \cos(\theta_Y) \quad (1.2)$$

Here, the  $\theta_W$  is defined as the most stable apparent contact angle and  $r$  is the roughness ratio. The roughness ratio is defined as the ratio of true area of the solid surface to the apparent area. The Wenzel equation only applies to homogeneous surfaces. To relate the APCA with the ACCA on a heterogeneous surface, like the one mentioned in this report, the right equation is the Cassie-Baxter equation. A heterogeneous surface consists of different materials, resulting in a varying surface tension and Young's contact angle  $\theta_Y$ . The Cassie-Baxter equation (1.3) takes this into account and uses these angles to determine the resulting macroscopic contact angle  $\theta_{CB}$ . The Cassie-Baxter equation for a two-component surface is given by:

$$\cos(\theta_{CB}) = f_1 \cos(\theta_{Y_1}) + f_2 \cos(\theta_{Y_2}) \quad (1.3)$$

Here,  $\theta_{CB}$  represents the Cassie-Baxter angle for a heterogeneous surface. Young's contact angle for the two different materials are given by  $\theta_{Y_1}$  and  $\theta_{Y_2}$  and  $f_1$  and  $f_2$  show the ratio of the areas of the two materials with respect to the total wetted area. The Cassie-Baxter equation calculates the contact angle by using a weighed average of the different contact angles determined with Young's equation (1.1).

## 1.2 Hydrophobic vs. hydrophilic

Hydrophobic materials are difficult to wet, they repel water. The cause lies on the molecular level, hydrophobic materials have apolar bonds and water has polar bonds, which causes water molecules to notice a stronger attraction to other water molecules than to the hydrophobic surface. A deposited droplet wants as little contact with the surface as possible, resulting in a very convex shape with large contact angles[6]. Hydrophilic materials are the opposite, they are easy to wet. A deposited droplet will be smeared over the surface to have as much contact with it as possible. This will result in significantly smaller contact angles compared to contact angles on hydrophobic materials. The difference between a hydrophobic and a hydrophilic surface can also be seen in Figure 1.2.

## 1.3 Advancing and receding edge

When more and more liquid is added to a droplet that lies on a surface, the contact angle will continuously increase but the contact line remains the same, which means that the droplet stays static. The angle at which the contact line also starts moving is the advancing contact angle (ACA). The other way around, taking liquid away, the contact line will remain constant but the contact angles will decrease. The angle at which the contact line starts to move is the receding contact angle (RCA). These angles are unique for the liquid being used and a specific surface. The difference between the advancing and receding contact angle is known as contact angle hysteresis. Reasons for hysteresis can be surface heterogeneity and surface roughness.

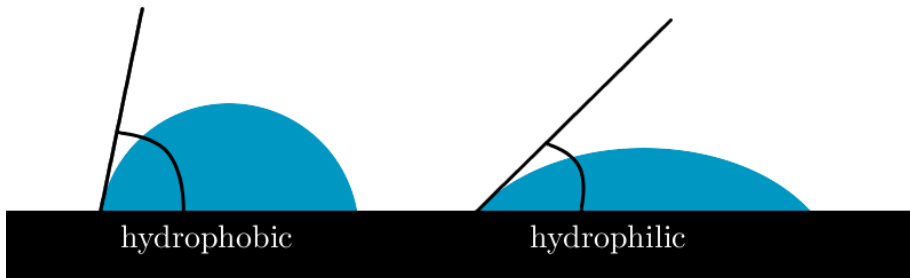


Figure 1.2: A droplet deposited on a hydrophobic and hydrophilic surface. The angle between the surface and the tangent is the contact angle. The contact angle for the hydrophobic surface is larger than the contact angle for the hydrophilic surface.

## 1.4 Energy gradients

On a surface with an energy gradient a droplet will move from the more hydrophobic to the more hydrophilic surface. This phenomenon is due to energy minimization[4]. The droplet will move to the surface with a higher surface energy to decrease the total energy. This can also be seen in Figure 1.3.

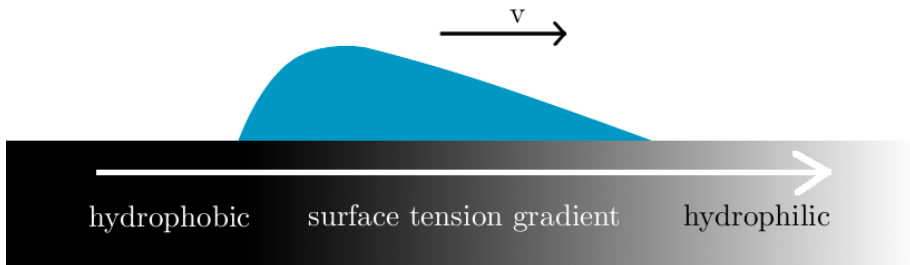


Figure 1.3: Schematic representation of a droplet deposited on a sample with a surface tension gradient. The droplet will move from the hydrophobic to the hydrophilic part.

This movement can be described by Young's force formula.

$$dF_Y = \gamma_{LF}(\cos(\theta_{Ad_1}) - \cos(\theta_{Re_2}))dx \quad (1.4)$$



With the  $\theta_{Ad_1}$  being the advancing contact angle on the front of the droplet and  $\theta_{Re_2}$  being the receding contact angle on the back of the droplet.

For the droplet to move, the difference between the ACA and RCA should be less than ten degrees. A energy gradient can be constructed on a surface by making different patterns of hydrophobic and hydrophilic materials. The hydrophobic material used is Per-FluoroDecylTrichloroSilane (PFDTs) and the hydrophilic material used is silicon dioxide ( $\text{SiO}_2$ ). To describe the ratio between the widths of the different materials, the parameter  $\alpha$  is defined to be[2]:

$$\alpha = \frac{W_{PFDTs}}{W_{SiO_2}} \quad (1.5)$$

A high value means a relatively hydrophobic material and a low  $\alpha$  equals a more hydrophilic material.

## 1.5 Forces

There are three forces involved in the movement of the droplet on the surface, the motive force ( $F_Y$ ) and the opposing hysteresis force ( $F_{Hys}$ ) and viscous drag force ( $F_\eta$ ) citeYang. The summation of these forces gives the acceleration of the droplet:

$$\sum F = F_Y - F_{Hys} - F_\eta = ma \quad (1.6)$$

The first of these three is the motive force due to Young's imbalance caused by the energy gradients. The motive force for a spherical droplet can be expressed as[5]:

$$F_Y = -\frac{d\Delta G}{dx} \cong \pi R^2 \gamma_{LG} \left( \frac{d \cos(\theta)}{dx} \right) \quad (1.7)$$

This force acts as the driving force,  $\Delta G$  is the difference in free energy,  $dx$  the difference in position,  $R$  is the radius of the wetted area of the droplet and  $\theta$  is the contact angle, which depends on the position.

The second is the force due to hysteresis, described by[3]:

$$F_{Hys} = \gamma_{LG} \int (\cos(\theta_{Ad_1}) - \cos(\theta_{Re_2})) dy \quad (1.8)$$

The third force is the viscous drag force, which can be described by:

$$F_\eta = 3\eta\pi RV \int_{x_{min}}^{x_{max}} \frac{dx}{\xi(x)} \quad (1.9)$$

Here,  $F_\eta$  is the force due to viscous drag,  $\eta$  is the viscosity of the fluid,  $\xi(x)$  is the height of the droplet and  $x_{max}$  and  $x_{min}$  are two cutoff lengths. For the droplet to move, the driving force should be greater than the drag and the hysteresis force combined. The velocity with which the droplet shall move is predicted to be linearly dependent to the viscosity of the droplet.

# Chapter 2

## Experimental aspects

The surface patterns used in the experiments consist of alternating hydrophobic and hydrophilic stripes on a silicon wafer. The hydrophilic stripes are the bare  $\text{SiO}_2$  surface and the hydrophobic stripes are self assembled mono-layers of 1H,1H,2H,2H- perfluorodecyl-trichlorosilane (PFDTS). Patterns with different surface energies are formed by varying the width of the stripes.

### 2.1 Pattern creation

The patterns can be created using standard clean room facilities, by using photo lithography. The clean silicon wafers are coated with a positive photo-resist. The photoresist layer is then exposed through a mask that has the desired pattern. The exposed parts of the photoresist are removed by a developer. The remaining photoresist is hard-baked and will protect the areas covered by it during the next step in the process, which is the chemical vapor deposition (CVD) of the PFDTS. After the CVD of the PFDTS the last part of the photoresist is washed off, leaving behind the desired patterned surface.

### 2.2 Individual patterns

To investigate the process of droplet movement on surfaces with a wettability gradient, several patterns with different gradients are constructed on one single wafer. An example of a patterned surface is given in Figure 2.1, the array shown is F1. The common feature for all these different patterns is the hydrophobic PFDTS rectangle on which the droplets are deposited. The dimensions of these PFDTS rectangle are  $2000 \mu\text{m} \times 4500 \mu\text{m}$  for most of the patterns and  $1500 \mu\text{m} \times 4500 \mu\text{m}$  for the E series(See appendix A). The size of this rectangle has to be larger than the diameter of the wetted area of the droplet. For a  $2 \mu\text{l}$  droplet of 1-decanol, the diameter of the wetted area on PFDTS is around  $2.8 \text{ mm}$ , which is larger than the width of the PFDTS rectangle. This is due to the fact that the wafer used was designed to work with water droplets, which have a smaller wetted area. The width of this first rectangle has to be bigger than the diameter of the wetted area, because otherwise the droplet will feel both the patterned, partial hydrophobic, surface and the unpatterned, hydrophilic, surface. This will result in a movement of the droplet straight onto the bare  $\text{SiO}_2$  surface. Next to the first, unpatterned PFDTS rectangle, rectangles

are created with a positive gradient in surface energy, resulting in the movement of a droplet over the consecutive patterns.

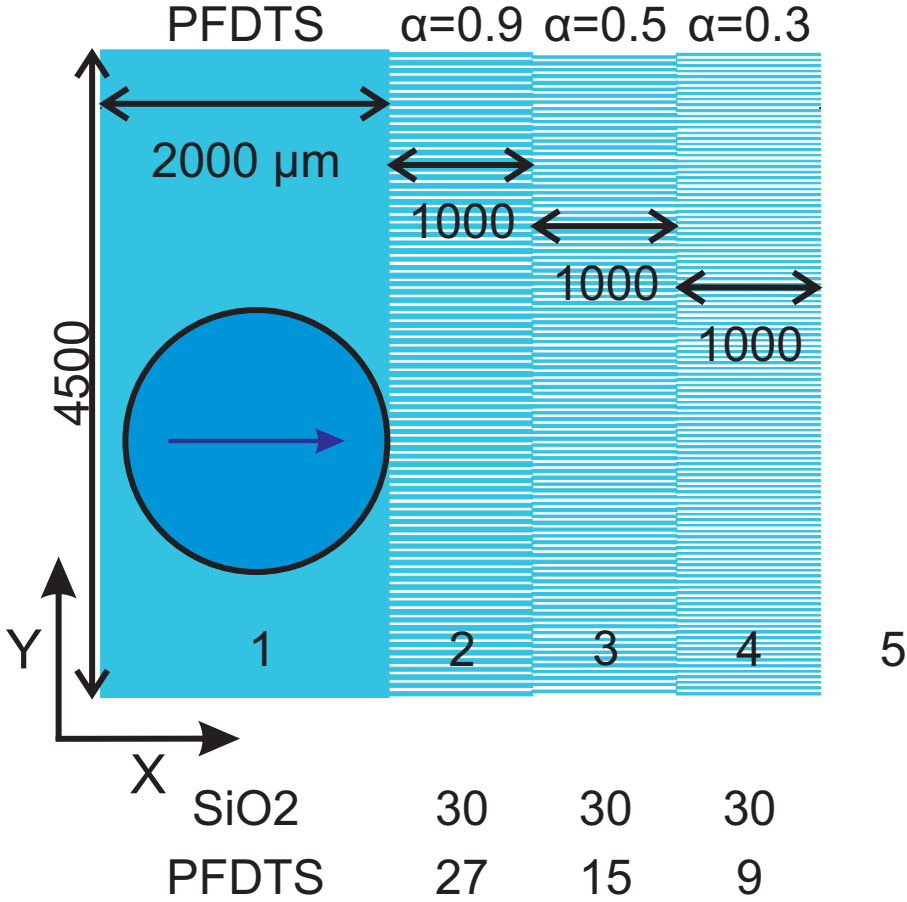


Figure 2.1: A standard gradient array. The blue lines represent the hydrophobic PFDTs stripes and the white lines are the hydrophilic SiO<sub>2</sub> surface. Part 1 is the pure PFDTs rectangle, part 2 is the first striped pattern, part 3 is the second striped pattern, part 4 is the third striped pattern and part 5 is the bare SiO<sub>2</sub> surface[7]

### 2.3 The dimensionless parameter $\alpha$

The relative hydrophobicity of a pattern is given by the dimensionless parameter  $\alpha$ , which is defined to be the width of the PFDTs stripes divided by the width of the SiO<sub>2</sub> stripes, see equation 1.5. The parameter  $\alpha$  is also a good indicator of the surface energy. A low  $\alpha$  means that the width of the SiO<sub>2</sub> stripes is larger than the width of the PFDTs stripes, meaning a hydrophilic surface. The other way around, a high  $\alpha$  means that the width of the PFDTs stripes is larger, resulting in a more hydrophobic surface. In Figure 2.1 it is seen that a single pattern consists of a PFDTs rectangle, followed by three striped patterns. These three patterns all have equally wide SiO<sub>2</sub> stripes, but different PFDTs

stripe widths and thus different  $\alpha$ . For all patterns one of the widths is fixed, while the other width varies. For the pattern of Figure 2.1 the width of the SiO<sub>2</sub> stripes is fixed at 30  $\mu\text{m}$ , while the width of the PFDTs stripes decreases from 27  $\mu\text{m}$  to 9  $\mu\text{m}$ . For all the different patterns on the wafer, the  $\alpha$  of a pattern is smaller than the  $\alpha$  of the preceding pattern. This means that the total pattern, consisting of the PFDTs rectangle and the three striped patterns, has a gradient in surface energy. A droplet deposited on the PFDTs rectangle will spread and will eventually probe the border with the striped surface that has a higher surface energy. The droplet will move over the border to lower its free energy.

## 2.4 Different rows

There are different patterns made on one silicon wafer, grouped in rows. An overview of the whole wafer is given in Figure 2.2. As can be seen in the figure, most of the wafer consists of the hydrophilic SiO<sub>2</sub> surface. The wafer can be divided into twelve rows, each row with one variable that changes in a controlled way. This renders the possibility to see how measurable parameters like speed, contact angle, etc. depend on the underlying  $\alpha$  and absolute stripe width.

Row A contains two patterns consisting of alternating stripes, but without a gradient. These patterns are not used in this experiment. Row B consists of four arrays, the width of the PFDTs stripes is the controlled variable. The sequence of  $\alpha$ 's of the different striped patterns and the width of the individual patterns is kept equal. Row C contains 6 arrays with the same  $\alpha$  sequence, but a variable length of the individual patterns, as can be seen in Figure 2.2. Row D also has 6 arrays with an equal  $\alpha$  for the first two patterns, but a variable  $\alpha$  for the third pattern. Row E has 8 arrays, each with the same  $\alpha$  sequence, but a variable SiO<sub>2</sub> stripe width. The F row is almost the same as the E row, only the length of the patterns on the E row is 700  $\mu\text{m}$ , while the length of the patterns on the F row is 1000  $\mu\text{m}$ . The G-series only has two striped patterns and the variable is the  $\alpha$  of the 1st pattern. In row H the  $\alpha$  of the 1st pattern as well as the  $\alpha$  of the 2nd pattern changes. The I-series has a constant value of  $\alpha$  for the 1st and the 3rd pattern, but the  $\alpha$  of the 2nd pattern varies. The J-series only has two striped patterns, and this time the difference between the  $\alpha$ 's of the patterns is constant, 0.2, while the absolute  $\alpha$ 's vary. Row K is equal to row J, only with a difference between the  $\alpha$ 's of the two striped patterns of 0.3. The L-series only has two arrays with a single striped pattern that can be used for reference. A complete overview of the lengths, PFDTs and SiO<sub>2</sub> stripe widths and  $\alpha$ 's of the different arrays on the wafer is given in appendix A.

## 2.5 Multiple wafers

For more accurate measurements, three wafers with the same arrays were used. In order to make a distinction between the wafers, they are numbered. W1 refers to the first wafer, W2 to the second wafer and W3 to the third wafer. The layers of PFDTs as well as the quality of the SiO<sub>2</sub> surface varies, leading to different contact angles and different speeds of the droplets. In this report, only measurements were done with W3 as W1 broke, which rendered it useless, and W2 did not function due to a low difference between the contact angles on the PFDTs and the SiO<sub>2</sub>.

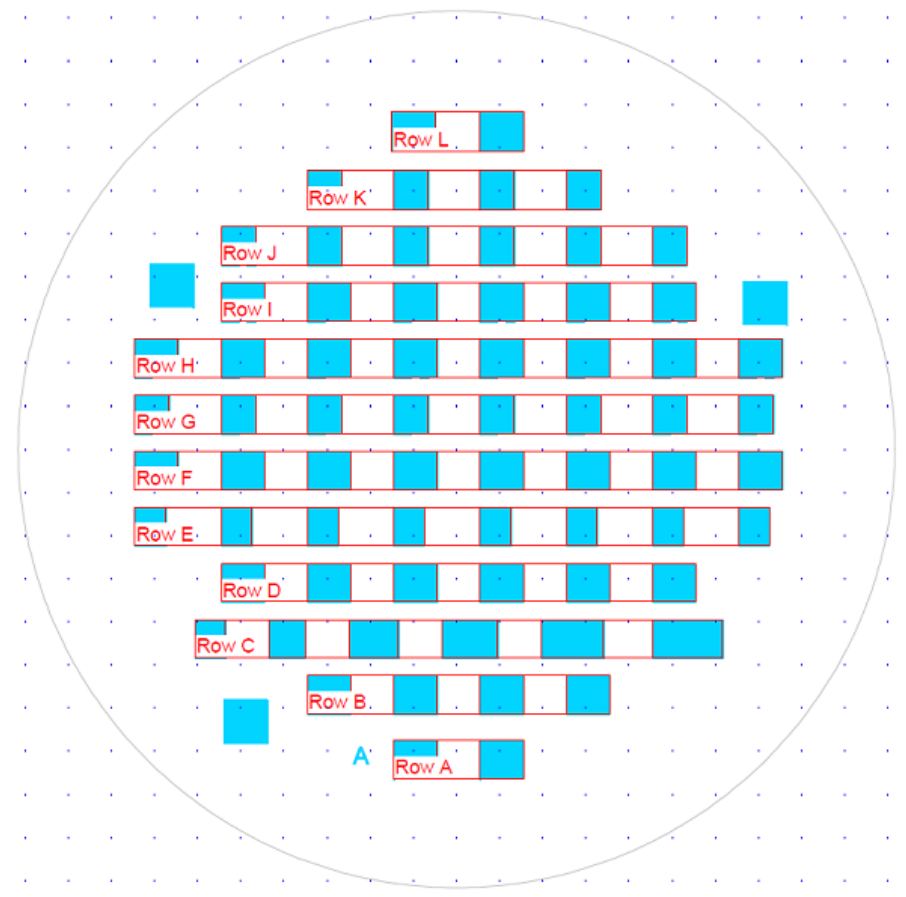


Figure 2.2: Schematic overview of the entire wafer, which can be divided into several rows[7].

## 2.6 Droplet deposition and droplet composition

Droplets with a volume of  $2 \mu\text{l}$  are created using a computer-controlled syringe. The droplets are suspended below the syringe prior to deposition. This minimizes the contribution of the kinetic energy from the droplet formation on the process. The droplet is then deposited on the surface and it will start spreading on the first PFDTs rectangle. The liquid used for the droplets is decanol and, unlike water, decanol does not detach from the needle on its own. Only once the needle is manually retracted from the surface, the receding edge of the droplet will start moving over the patterns. The surface tension for decanol at standard conditions is  $12.4 \text{ mN/m}$ , while the surface tension for water at standard conditions is  $73.4 \text{ mN/m}$ . The viscosity of decanol ( $0.041 \text{ Pa s}$ ) is twelve times the viscosity of water ( $0.001 \text{ Pa s}$ ).



# Chapter 3

## Analysis

The experimental data used for the analysis are the movies, made with the high-speed camera, of the droplet moving across the patterns. After analysis of the movies, the extracted information about the droplet movement includes position of the edges, speed of the edges, position of the center, speed of the center and the contact angles of the droplet as a function of time. These features depend on the pattern over which the droplet is moving and comparison of several patterns can be done once the data is extracted.

### 3.1 Input

The program used to analyze the movies is Matlab, making a fairly quick analysis of the movies possible. The movies are loaded into Matlab as separate images, one image per frame, and then analyzed. The camera used for the recording of the movies is a FASTCAM SA3 model 120K-M2. In order for MATLAB to correctly process the images, the contrast needs to be as high as possible. This means that the image should almost be solely black and white and should contain little gray. With the experimental conditions as described in this report this means that the background should be white and the droplet and the needle should be black. A high-speed camera only has a limited internal storage, which means that the movies can only be a few seconds long. However, the whole movement of the droplet can take up to thirteen seconds, making a well-fitted resolution of the movie important.

### 3.2 Matlab script

The MATLAB script works by loading the images and converting them into solely black and white (dual-tone) images, giving a matrix of zeros and ones. A zero corresponds to a black pixel and a one corresponds to a white pixel. Edge detection can be done by finding the transition from ones to zeros in the image. The positions of both the front and the back of the droplet are calculated by taking the transition point at the baseline. The baseline is the line that represents the surface and has to be entered manually, by clicking the broadest part of the droplet. The positions of the edges of the droplet are now known, but need to be converted into millimeter. This is done by using the syringe as a reference, since the syringe width is known to be 0.26 mm, from which the pixel-mm ratio can be calculated.

### 3.3 Positions and velocities

The starting point of the center of the droplet also needs to be calculated, this is done by taking the center of the needle as the center of the droplet at the starting time. This can be defended by the fact that the droplet will spread out radially first and the center of the droplet is thus on the same axis as the center of the needle. The positions of the left and right border and the center of the droplet are now known for all individual frames. When the positions of these points are compared between all the frames, the speeds can be calculated. The distance traveled between two consecutive frames is known and the time between these frames is known to be the inverse frame rate, and thus the speed can be calculated.

### 3.4 Program shortcomings

The program has some shortcoming, not serious enough to render the program useless, but they should be named nonetheless. The program assumes the baseline to be completely horizontal, while this is not always true. During the measurements the camera can become slightly tilted, due to movement of the camera and table. This means the baseline is not completely horizontal anymore and there is thus an error in the contact angles. The droplet out of itself does not detach from the needle, meaning the needle is also included in the fit of the droplet, leading to wrong contact angles. This problem can be partially solved however, by selecting the top of the droplet very precisely. The light is also a major reason for errors in the data. Sometimes a part of the droplet or a part of the needle is over- or underexposed, giving a wrong pixel-mm ratio and an incorrect droplet shape. This has to be accounted for in further error corrections. Contact angles for the droplet on the third and final pattern are off, because the droplet will start spreading radially on the third pattern, causing it to move out of focus, which influences the gray transition area.

### 3.5 Error bars

To take into calculation the errors and inaccuracies, an absolute or relative error should be calculated. However, since most measurements were done in duplicate, the standard deviation should give a good indication of the size of the error. As can be seen in the data graphs in the chapter "Results and discussion", the standard deviation between two or three measurements is very large compared to the values of the measurements. This means that the values given by measurements differ greatly. This can be explained by the fact that the wafer collects dust between measurements, something which is very hard to correct. The droplet does not detach from the needle automatically, which means the needle has to be detached manually, giving rise to new inaccuracies. However, trends are still visible and the measurements can thus be used for qualitative purposes, indicating positive or negative relations or no relation at all.



# Chapter 4

## Results and discussion

The results of the experiments are sorted by row and thus by variable. For each of the rows, the speed of the advancing edge over the three striped patterns, the speed of the receding edge and the speed of the droplet center are plotted as a function of the controlled variable. For each row this results in three different graphs, all with three data series for the different striped patterns. Also, a plot is made of the exit time vs. the controlled variable. Finally, a plot of the speed of the advancing edge on the first pattern as a function of the distance to the first border is made. Only the relevant graphs are shown in this report.

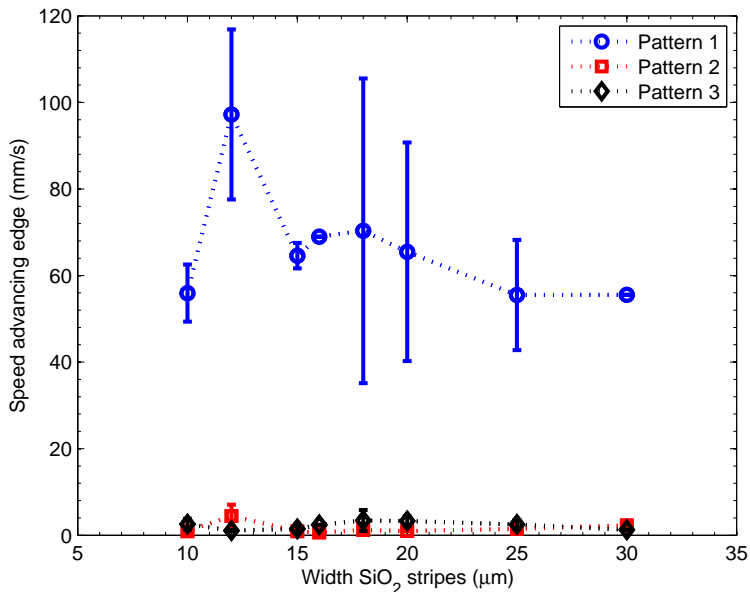


Figure 4.1: Graph displaying the speed of the advancing edge as a function of the absolute SiO<sub>2</sub> stripe width, for the E row.

In Figure 4.1, it can be seen that there is a large scatter of the speed of the advancing edge on the first pattern. This is true for all rows and is due to the fact that the droplet is still attached to the needle. As long as the droplet is attached to the needle, the movement

is only slightly influenced by the sub-lying pattern. Since the droplet does not detach automatically, the moment the droplet starts moving, because of the sub-lying pattern, is influenced by the human interaction of detaching the needle. This results in large scatter of the values and this is the reason for not showing the speed of the advancing edge on the first pattern.

## 4.1 Regimes

The movement of the droplet can be subdivided into four regimes. An image of these four regimes is seen in Figure 4.2. The first regime is characterized by the inertial spreading of the droplet. It begins when the droplet makes contact with the surface and ends once the needle is detached from the droplet. In this stage, droplet motion is not mainly dependent on the patterned surface beneath the droplet, since the influence of the needle is much larger. The second regime starts here and ends once the receding edge of the droplet is pinned at the border between the PFDTs rectangle and the first striped pattern. In this regime, the droplet elongates along the direction of motion. The droplet does not move in the perpendicular direction, because of a too large energy border in the transverse direction, caused by the PFDTs. The third regime starts after this and ends once the advancing border of the droplet reaches the  $\text{SiO}_2$  surface. This causes the receding edge to release from the border. The third regime is characterized by further elongation of the droplet. The fourth regime starts once the advancing edge of the droplet reaches the  $\text{SiO}_2$  surface. The droplet is no longer confined in the transverse direction and radial spreading takes place. The fourth regime ends once the whole droplet is on the  $\text{SiO}_2$  surface.

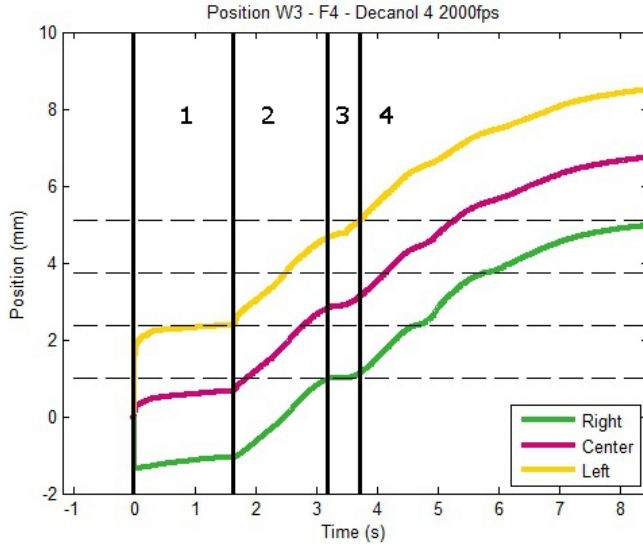
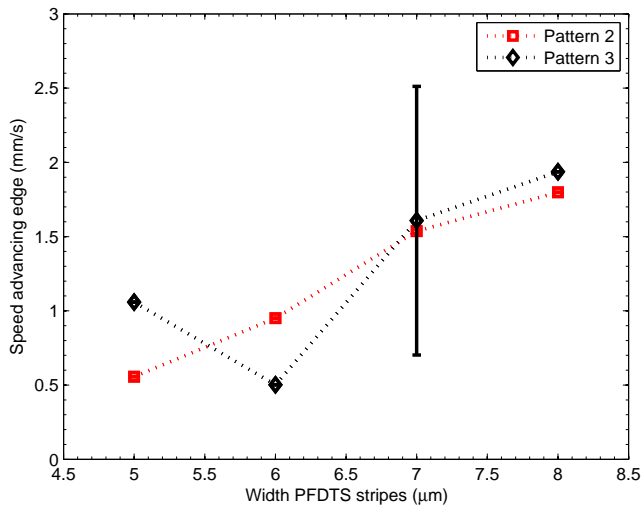
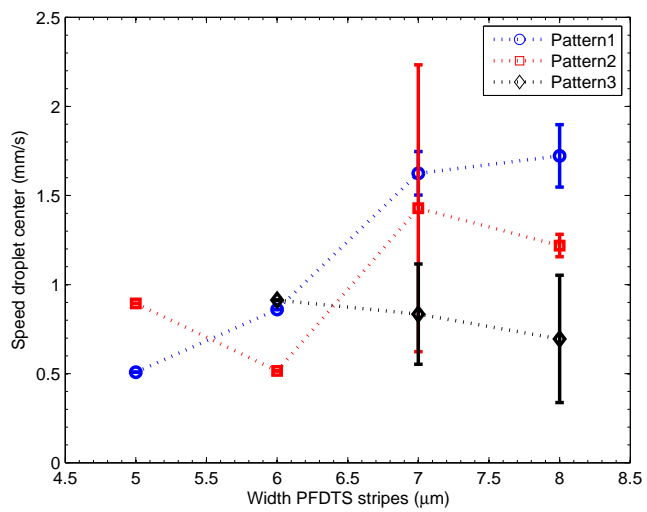


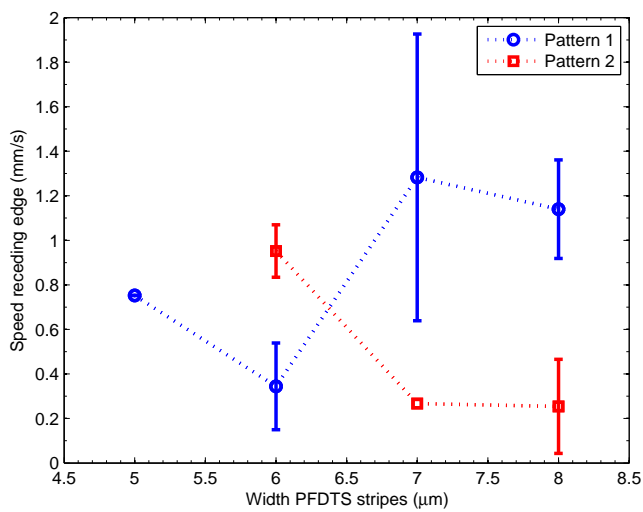
Figure 4.2: A position versus time graph of array F4. Shown in the image are the four regimes. The areas between the two lines indicated by 1, 2, 3 and 4 are respectively the first, second, third and fourth regime.



(a) Advancing edge



(b) Receding edge



(c) Center of the droplet

Figure 4.3: B row. Speed of the advancing edge (a), the receding edge (c) and the center of the droplet (b) as a function of the PFDTs stripe width

## 4.2 B row

The controlled variable for the B row is the absolute width of the PFDTs stripes. For all three striped patterns, the ratio between the PFDTs and the SiO<sub>2</sub> stripes remains the same, but the absolute width of the PFDTs stripes varies in a controlled way. The widths of the PFDTs stripes for the B row are given in Appendix A.

The absolute width of the PFDTs stripes has no measurable influence on the speed of the advancing edge on the first pattern and on the speed of the receding edge and the droplet center on the first and second striped pattern, as can be seen in Figure 4.3. This can be explained by the time of release, the moment the droplet detaches from the needle. On the first two patterns, the droplet is still attached to the needle, which restricts the speed.

The speed of the advancing edge on the second and third striped pattern does depend on the absolute width of the PFDTs stripes, as seen in Figure 4.3(a). As the width of the PFDTs stripes increases, the speed of the advancing edge also increases. The droplet tends to move only on the hydrophilic (SiO<sub>2</sub>) stripes and as the width of the PFDTs stripes increases the width of the SiO<sub>2</sub> stripes does too. The total number of stripes on which the droplet moves decreases, making it easier for the droplet to move around and thus increasing the speed. When fluid flows through a canal (the SiO<sub>2</sub> stripe between the two hydrophobic stripes functions as a canal), there is friction between the fluid and the edges of the canal, causing the velocity to decrease. With an increasing width of the canal, the relative surface between the fluid and the canal decreases, decreasing the influence of the friction. This explains why the velocity of the advancing edge increases as the absolute width of the PFDTs stripes increases; because the width of the SiO<sub>2</sub> stripes also increases.

## 4.3 C row

The length of the patterns is different for the arrays in the C row. As the total length of the array grows, the droplet will not be able to move over the entire pattern. The steps in surface energy are too far apart to 'pull' the droplet across. The relevant results for the C row are shown in Figure 4.5.

As can be seen in Figure 4.5(a) the speed of the advancing edge on the first pattern seems to decrease as the length of the first pattern increases. On the first pattern, the droplet is still attached to the needle, which heavily influences the speed of the advancing edge.

Figure 4.5(b) shows the exit time, the time it takes the advancing edge to leave the last striped pattern, as a function of the length of the patterns. It should be stated that not only the length of the first pattern, but also the length of the second and third pattern changes (however, the length of the first, second and third pattern are always the same for one array), as can be seen in Appendix A. The exit time increases as the length of the striped patterns increases. If the length of the individual patterns increases, there is a equal surface energy difference on a larger distance, which leads to a decrease of the gradient. As stated in formula (1.6) the surface energy gradient has a positive influence on the motive force on the droplet. So, if the surface energy gradient decreases, so does the motive force, resulting in slower droplet movement. Thus, the total distance the advancing edge needs to cross becomes larger while the surface energy gradient decreases, combining these two explains the higher exit time. The C row contains six patterns, with increasing pattern lengths. Pattern five and six are not taken into account, because the droplet does not reach the end of the pattern but stays on it. Here, the distance between the patterns

is too large. Pattern four can also be neglected, but for a different reason. As can be seen in Figure 4.4, the detachment of the droplet happens when the advancing edge is already at the end of pattern three. The detachment provides a speed increase making sure the droplet reaches the end of the pattern very quickly, resulting in a very small exit time.

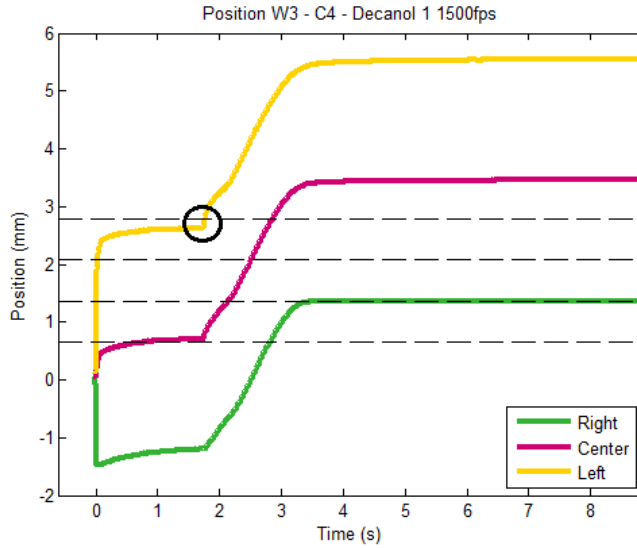
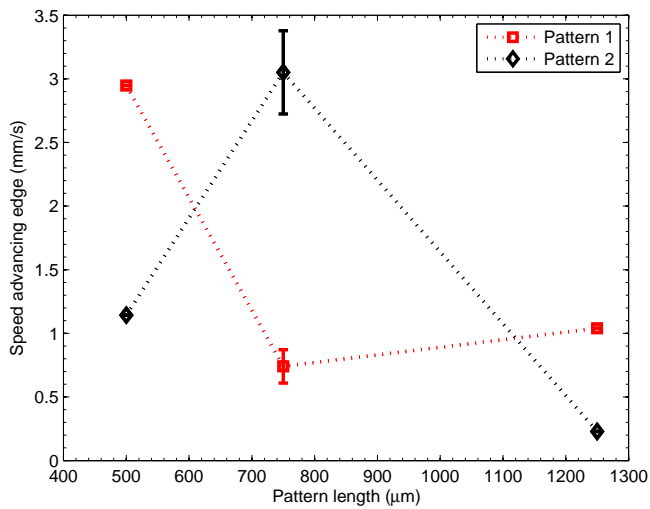
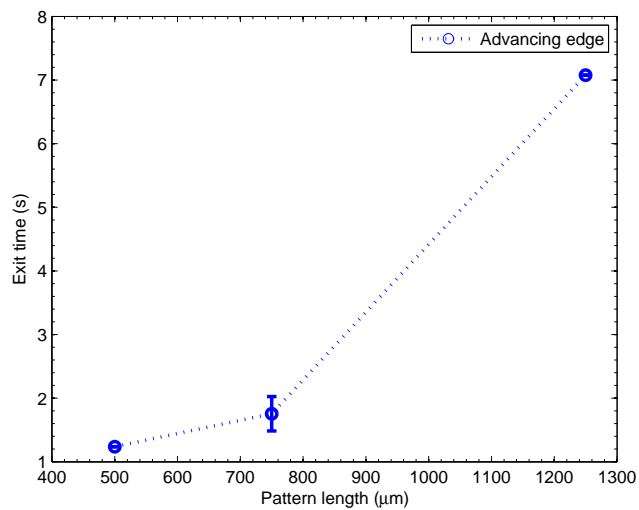


Figure 4.4: A position versus time graph of array C4. Here, the dashed lines represent the 4 borders on the array. The black circle shows the position where the droplet is detached from the needle. As can be seen, the detachment takes place at the end of the third pattern.

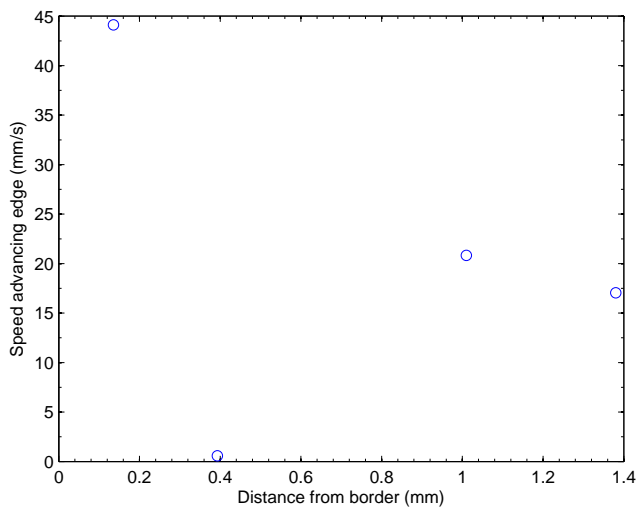
The last graph, Figure 4.5(c) displays the speed versus the distance between the center of the droplet and the first striped pattern at the deposition time. From the graph, it can be seen that the distance to the first border has no influence on the speed. This is because the droplet first spreads out radially, while it is still attached to the needle, and only once the needle is removed the droplet will start moving across the patterns.



(a) Advancing edge



(b) Exit time



(c) Distance

Figure 4.5: C row. Speed of the advancing edge as a function of the length of the striped patterns (a), Exit time of the advancing edge as a function of the length of the striped patterns (b) and the speed on the first pattern as a function of the distance between the center of the droplet and the edge of the first striped pattern at  $t=0$  (c).

## 4.4 D row

On the D row, the  $\alpha$  of the third pattern changes. The  $\alpha$  changes from 0.125 to 0.4375, the lower  $\alpha$ 's corresponding to striped patterns with relatively wide SiO<sub>2</sub> stripes and the higher  $\alpha$ 's corresponding to patterns with wide PFDTS stripes. The array with an  $\alpha$  of the third pattern of 0.4375 is not shown in the graph because there were no good measurements of this array.

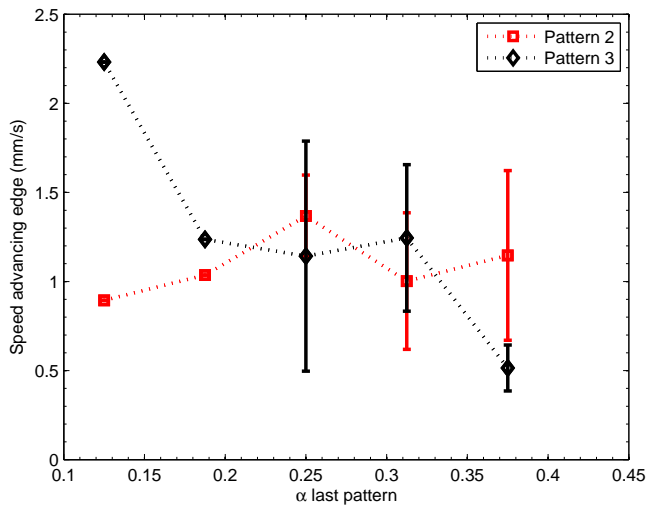
The two main results for the D row are given in Figure 4.6. Figure 4.6(a) shows the speed of the advancing edge as a function of the  $\alpha$  of the third striped pattern. The speed of the advancing edge decreases as the  $\alpha$  increases. As the  $\alpha$  increases, the third striped pattern will have relatively wider PFDTS stripes, resulting in more hydrophobic patterns. The droplet will move slower if the third striped pattern becomes more hydrophobic, which can be partly explained by the decrease in surface energy gradient between the second and third striped pattern. A droplet will tend to take on a more convex shape on a hydrophobic surface, meaning that the advancing and the receding edge will be close together. The receding edge of the droplet is pinned at the edge between the PFDTS surface and the first pattern. While the third pattern has a small enough  $\alpha$ , the advancing edge will move over the third pattern, at the same time detaching the receding edge. But when  $\alpha$  gets larger, making the third pattern more hydrophobic, the motive force on the advancing edge becomes smaller and the droplet slows down. Only when the advancing contact angle is small enough will the receding edge depin. As a result of this detachment the speed of the advancing edge increases, passing the speed increase on to the receding edge, and the advancing edge will cross the fourth border and reach the SiO<sub>2</sub> surface.

The exit time of both the advancing edge and the center of the droplet also depends on the  $\alpha$  of the third striped pattern, as can be seen in Figure 4.6(b). The exit time of both tends to increase with an increasing  $\alpha$  of the third striped pattern. This can also be explained by looking at Figure 4.6(a). A increasing  $\alpha$  leads to lower speeds of the advancing edge. The total distance the advancing edge needs to cross remains equal, but the velocity decreases, leading to higher exit times. The exit time of the center of the droplet also decreases because of this. The receding edge is pinned at the border between the second and third pattern and thus does not contribute to the exit time of the center of the droplet.

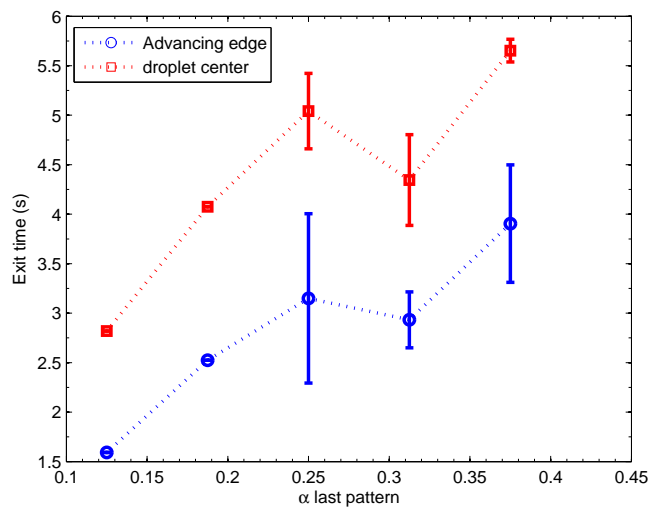
## 4.5 E row

The E row is different from the other rows in the fact that the length of the striped patterns is not 1 mm, as for the other rows, but 0.7 mm. The patterns are shorter, which leads to a higher overall surface energy gradient and a shorter distance for the droplet to move across. The width of the SiO<sub>2</sub> stripes also changes in a controlled way. For all three striped patterns, the ratio between the PFDTS and the SiO<sub>2</sub> stripes remains the same, but the absolute width of the SiO<sub>2</sub> stripes varies in a controlled way. The widths 10, 12, 15, 16, 18, 20, 25 and 30  $\mu\text{m}$  are used.

The speed of the advancing edge is displayed versus the width of the SiO<sub>2</sub> stripes in Figure 4.7(a). As can be easily seen, the values scatter heavily. The E row has shorter striped patterns and also a shorter PFDTS rectangle on the beginning of the pattern, making droplet deposition more difficult. The advancing edge of the droplet has already crossed the first and most of the second striped pattern while the droplet is still attached to the needle. This gives rise to the large scatter of the speed of the advancing edge on the first pattern.



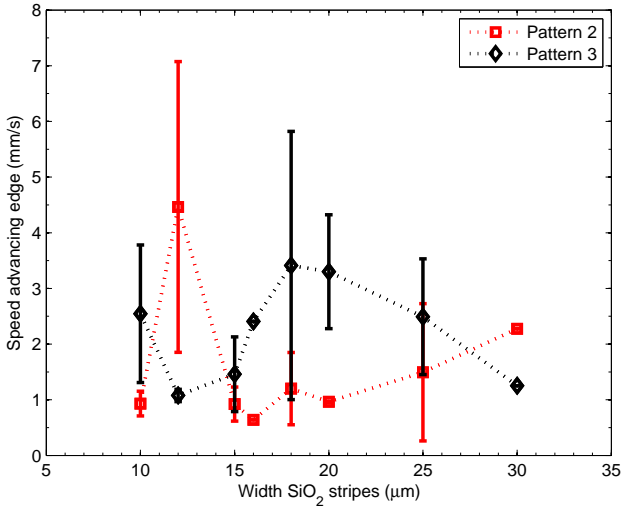
(a) Advancing edge



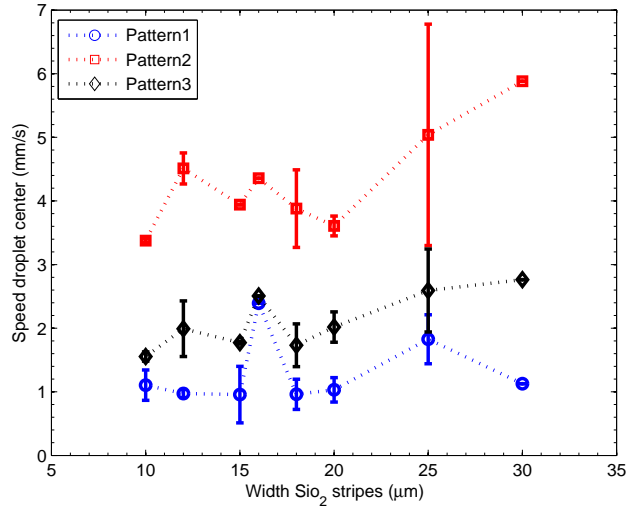
(b) Exit time

Figure 4.6: D row. Speed of the advancing edge as a function of the  $\alpha$  of pattern 3 (a), Exit time of the advancing edge and the center of the droplet as a function of the  $\alpha$  of pattern 3 (b)

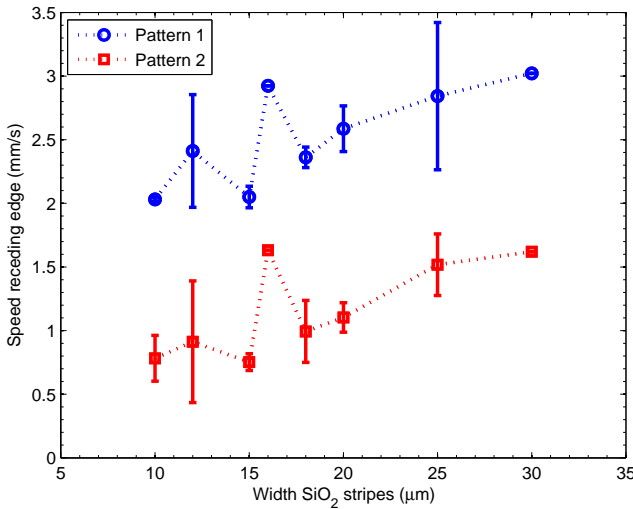




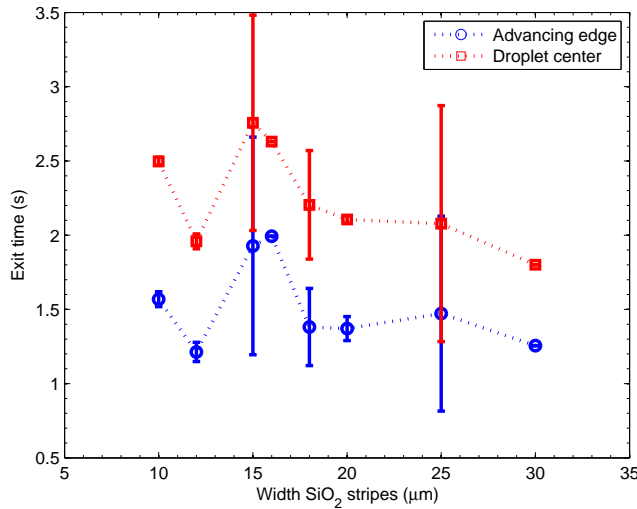
(a) Advancing edge



(b) Droplet center



(c) Receding edge



(d) Exit time

Figure 4.7: E row. Speed of the advancing edge as a function of the absolute width of the SiO<sub>2</sub> stripes (a), speed of the droplet center as a function of the absolute width of the SiO<sub>2</sub> stripes (b), speed of the receding edge as a function of the absolute width of the SiO<sub>2</sub> stripes (c), exit time of the advancing edge and the center of the droplet as a function of the absolute width of the SiO<sub>2</sub> stripes (d).

The advancing edge will move on the second pattern but will not cross over to the third pattern until the needle is detached, which means that the total time the advancing edge is on the second pattern is mainly determined by the time between droplet deposition and needle detachment.

Since this is a purely human influence, the needle needs to be detached manually, it is very difficult to say anything about the speeds of the advancing edge over the second pattern. As said before, the detachment of the droplet heavily influences the speed of the droplet. For this reason little can be said about the influence of the surface on the speed of the advancing edge over the third pattern as well.

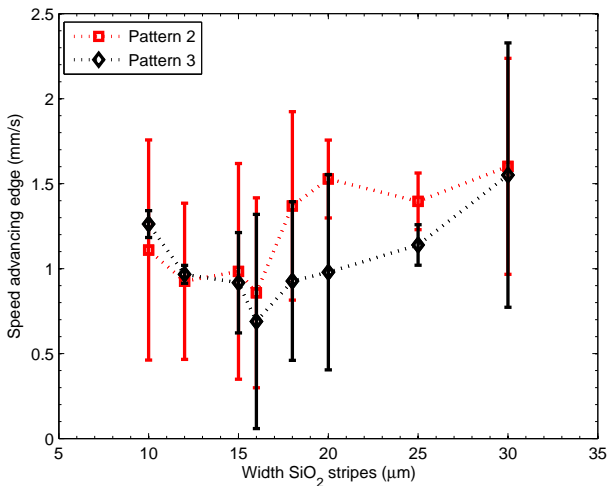
Figure 4.7(c) shows the speed of the receding edge as a function of the  $\text{SiO}_2$  stripe width. There is still a large scatter in the results, but an overall trend is visible. As the width of the ( $\text{SiO}_2$ ) stripes increases, the speed of the receding edge also increases. The  $\alpha$  of the striped patterns does not change with the changing  $\text{SiO}_2$  stripe width because the PFDTs stripe width also increases. So increasing the width of the  $\text{SiO}_2$  stripes also means increasing the width of the PFDTs stripes. The same situation can be seen in row B, where the width of the PFDTs stripes is the variable. The speed of the receding edge as a function of the PFDTs stripe width can be found in Figure 4.3. The increase in speed can be explained by the fact that the width of the  $\text{SiO}_2$  increases, meaning wider canals for the droplet to move through, as explained in paragraph 4.1.

Shown in Figure 4.7(d) is the exit time of the advancing edge of the droplet and the center of the droplet. Even though there is a large scatter, the exit time of the advancing edge seems to be independent of the stripe width of the  $\text{SiO}_2$  stripes. This can be explained by the fact that most of the movement of the advancing edge of the array happens when the droplet is still attached to the needle, reducing the influence of the surface beneath the droplet. The exit time of the center of the droplet seems to follow the same trend as the exit time of the advancing edge of the droplet. As the receding edge of the droplet stays pinned at the border between the second and third striped pattern, for all the measurements the exit time of the center of the droplet is determined by that of the advancing edge. However, the exit time of the advancing edge is heavily influenced by the time of detachment from the needle.

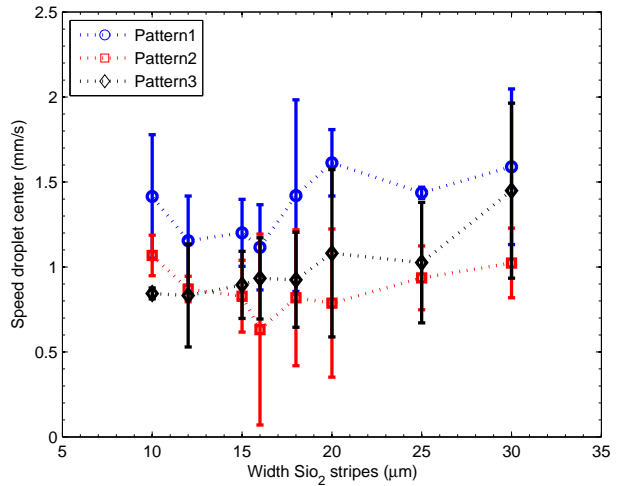
## 4.6 F row

The F row is equal to the E row except for the length of the striped patterns and the PFDTs rectangle, which is 1 mm for the F row, in contrast to 0.7 mm for the E row. Same as for the E row, the controlled variable for the F row is the width of the  $\text{SiO}_2$  stripes.

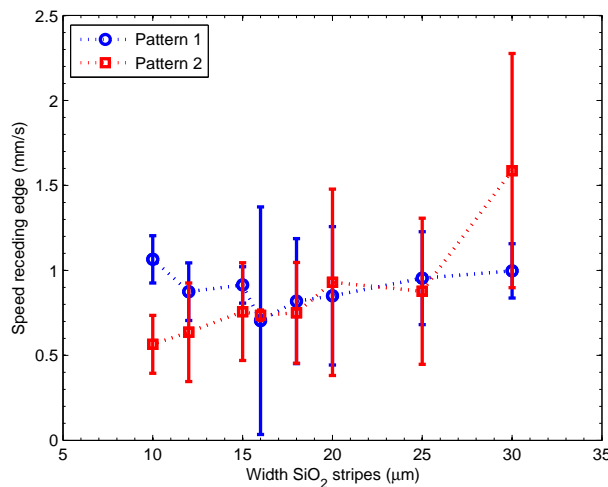
Figure 4.8(a) shows the advancing edge as a function of the width of the  $\text{SiO}_2$  stripes. Again, on the first pattern the droplet is still attached to the needle, giving rise to an enormous scatter of the speed on the first pattern. For this reason, the speed on the first pattern is not shown. For the second and third pattern however, a clear trend emerges; as the  $\text{SiO}_2$  stripe width increases, so does the speed of the advancing edge. This, once again, can be explained by the fact that the canals through which the droplet flows become wider, causing relatively less friction. The speed of the droplet center follows this same trend, as can be seen in Figure 4.8(b). For the first pattern, the speed of the receding edge does not seem to depend on the width of the  $\text{SiO}_2$  stripes. The speed of the receding edge on the second pattern increases as the stripe width increases, as can be seen in Figure 4.8(c). This too is explained by the widening of the canals as the  $\text{SiO}_2$  stripe width increases.



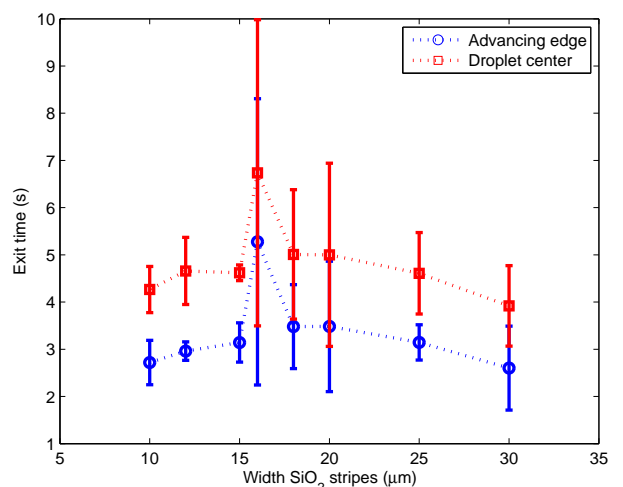
(a) Advancing edge



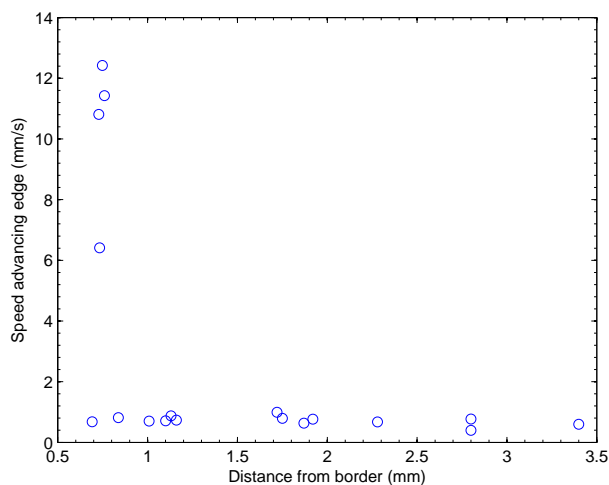
(b) Droplet center



(c) Receding edge



(d) Exit time



(e) Distance

Figure 4.8: F row. Speed of the advancing edge as a function of the absolute width of the SiO<sub>2</sub> stripes (a), speed of the droplet center as a function of the absolute width of the SiO<sub>2</sub> stripes (b), speed of the receding edge as a function of the absolute width of the SiO<sub>2</sub> stripes (c), exit time of the advancing edge and the center of the droplet as a function of the absolute width of the SiO<sub>2</sub> stripes (d), speed on the first pattern as a function of the distance between the center of the droplet and the edge of the first striped pattern at t=0 (e).

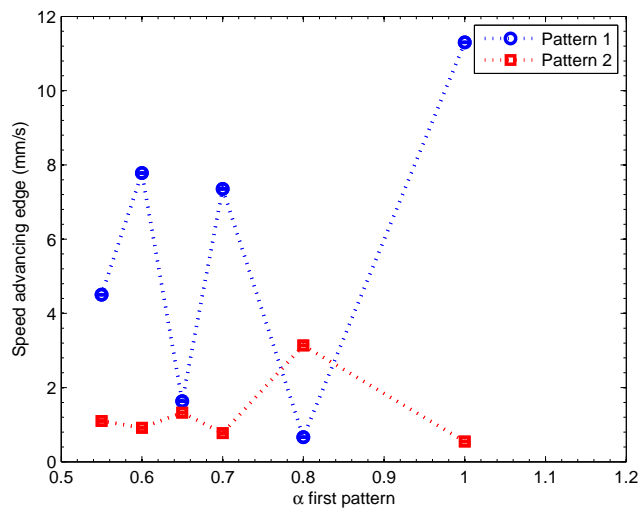
Figure 4.8(d) shows the exit time of the advancing edge and the center of the droplet. The exit time does not seem to depend on the width of the SiO<sub>2</sub> stripes, which is due to the large spread in speeds of the advancing edge on the first pattern. The speeds on the first pattern are higher than the speeds on the other striped patterns, so the scatter in the speeds on the first pattern explains the scatter in the exit times.

Figure 4.8(e) shows the speed on the first pattern as a function of the distance between the center of the droplet and the edge of the first striped pattern at the time of deposition. From the figure, this speed does not seem to depend on the distance from the border. This is because the droplet first spreads out radially, while it is still attached to the needle, and only once the needle is removed the receding edge of the droplet will start moving across the patterns.

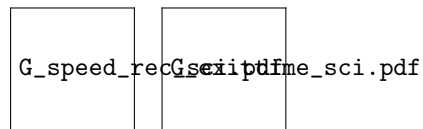
## 4.7 G row

The G row is similar to the D row, in the sense that the  $\alpha$  of one of the striped patterns changes. For the D row, it is the  $\alpha$  of the third pattern that changes, while for the G row the  $\alpha$  of the first pattern changes. Beside the changing  $\alpha$ , there is another difference that sets apart the G row. These arrays only have two striped patterns instead of three.

Figure 4.9(a) displays the speed of the advancing edge of the droplet versus the  $\alpha$  of the first striped pattern. The speed of the advancing edge on the first striped pattern fluctuates because the droplet is still attached to the needle and the speed on the first pattern depends on the time between deposition and the removal of the needle. These fluctuations also influence the speed of the advancing edge on the second striped pattern, although the fluctuations are smaller than for the first pattern. The speed of the advancing edge on the second striped pattern does not seem to depend on the  $\alpha$  of the first pattern. The second striped pattern is equal for all the arrays in row G, explaining the constant speed. The speed of the receding edge is shown in Figure 4.9(b). As can be seen, the speed of the receding edge increases as  $\alpha$  of the first pattern increases. An increasing  $\alpha$  means that the pattern is more hydrophobic, making the droplet wanting to take on a more convex shape. In order for the receding edge of the droplet to be closer to the advancing edge of the droplet, the receding edge of the droplet will move faster. Figure 4.9(c) shows the exit time of both the advancing edge and of the center as a function of the  $\alpha$  of the first striped pattern. The exit time of the advancing edge increases with an increasing  $\alpha$ , or in other words with a surface becoming more hydrophobic. As said before, this makes the droplet take on a more convex shape. In this case it means that the advancing edge of the border will move slower while the receding edge of the pattern will move faster. This shows in both Figure 4.9(b) and Figure 4.9(c).



(a) Advancing edge



(b) Receding edge (c) Exit time edge

Figure 4.9: G row. Speed of the advancing edge as a function of the  $\alpha$  of the first pattern (a), speed of the receding edge as a function of the  $\alpha$  of the first pattern (b), Exit time of the advancing edge of the droplet as a function of the  $\alpha$  of the first pattern (c)

# Chapter 5

## Conclusion

On the wafer, several different rows are created, all with arrays that have one variable that changes in a controlled way. This allowed for determination of the dependency of the motion of the droplet on these variables. These variables will be treated separately in this conclusion, for a clear overview.

First, the absolute width of the  $\text{SiO}_2$  or the PFDTs stripes can be changed, keeping the  $\alpha$  of the striped patterns constant. This is true for rows B, E and F. The influence of increasing the width of these stripes is that the droplet will move faster. This is a result of the larger width of the hydrophilic  $\text{SiO}_2$  canals the droplet moves through. For the advancing edge, this is seen in Figure 4.8(a) and for the droplet center this can be seen in Figure 4.8(c).

Second, the size of the individual striped patterns can be changed, as is done in the C row. A comparison between the E row and the F row can also be made. The E row is the same as the F row, except that the length of the striped patterns is  $700\ \mu\text{m}$ , while for the F row this length is  $1000\ \mu\text{m}$ . A shorter length of the individual patterns means that the droplet will move over a larger portion of the pattern while still being attached to the needle. This means that the motion of the droplet is mainly determined by the droplet being attached to the needle, not by the patterned surface beneath the droplet, resulting in the scatter seen in Figure 4.7(c). The length of the patterns also changes on the C row. When the length of the individual patterns becomes too large, the surface energy gradient will not suffice to move the droplet. This means that, in order to examine the influence of the patterned surface on the droplet motion, the length of the individual patterns should be optimized. Further research could investigate this length and optimize it.

Third, the  $\alpha$  of one of the striped patterns can be changed. This is done for the first pattern in row G and for the third pattern in row D. As seen in Figure 4.9(b) the speed of the receding edge increases as the  $\alpha$  of the first pattern increases. This can be explained by the surface becoming more hydrophobic, making the droplet contract. When the  $\alpha$  of the third pattern is increased, the speed of the advancing edge decreases. This can be explained by the fact the surface becomes more hydrophobic, decreasing the surface energy gradient between the second and third striped patterns. As the motive force is due to this gradient (equation 1.7), this explains the lower velocity of the advancing edge.

Interpreting the results was difficult and therefore there are some recommendations to be made. First of all, the fact that the droplet does not detach from the needle automatically gives rise to major errors. This might be solved by using a special coating on the outside of the needle, which is definitely worth the research. Another major improvement

could be made by increasing the number of arrays on one row. There are only between four and eight arrays on one row, making quantitative analysis difficult. By increasing the number of arrays or the number of wafers and decreasing the steps between the variables, the accuracy of the data could be improved.

# Bibliography

- [1] O. Bliznyuk. *Directional wetting on patterned surfaces*. PhD thesis, University of Twente, 2011.
- [2] O. Bliznyuk, E. Vereshchagina, E. Stefan Kooij, and Bene Poelsema. Scaling of anisotropic droplet shapes on chemically stripe-patterned surfaces. *Phys. Rev. E*, 79(4):041601, Apr 2009.
- [3] F. Brochard. Motions of droplets on solid surfaces induced by chemical or thermal gradients. *Langmuir*, 5(2):432–438, 1989.
- [4] Manoj K. Chaudhury and George M. Whitesides. How to Make Water Run Uphill. *Science*, 256(5063):1539–1541, 1992.
- [5] Susan Daniel and Manoj K. Chaudhury. Rectified motion of liquid drops on gradient surfaces induced by vibration. *Langmuir*, 18(9):3404–3407, 2002.
- [6] P.G. de Gennes, F. Brochard-Wyart, and D. Quere. *Capillarity and Wetting Phenomena: Drops, Bubbles, Pearls, Waves*. Springer, 2003.
- [7] H. P. Jansen. Energy gradient induced droplet dynamics on chemically stripe-patterned surfaces. Master’s thesis, University of Twente, 2010.
- [8] A. Marmur. Soft contact: measurement and interpretation of contact angles. *Soft matter*, 2:12–17, 2006.



# Appendix A

Table 1: B series

<b>Name</b>	B1	B2	B3	B4
Size PFDTs ( $\mu\text{m}$ )	2000	2000	2000	2000
Size S-P1 ( $\mu\text{m}$ )	1000	1000	1000	1000
$W_{SiO_2}$ ( $\mu\text{m}$ )	5,6	6,7	7,8	8,9
$W_{PFDTs}$ ( $\mu\text{m}$ )	<b>5</b>	<b>6</b>	<b>7</b>	<b>8</b>
$\alpha 1$	0,9	0,9	0,9	0,9
Size S-P2 ( $\mu\text{m}$ )	1000	1000	1000	1000
$W_{SiO_2}$ ( $\mu\text{m}$ )	10	12	14	16
$W_{PFDTs}$ ( $\mu\text{m}$ )	<b>5</b>	<b>6</b>	<b>7</b>	<b>8</b>
$\alpha 2$	0,5	0,5	0,5	0,5
Size S-P3 ( $\mu\text{m}$ )	1000	1000	1000	1000
$W_{SiO_2}$ ( $\mu\text{m}$ )	16,67	20,00	23,33	26,67
$W_{PFDTs}$ ( $\mu\text{m}$ )	<b>5</b>	<b>6</b>	<b>7</b>	<b>8</b>
$\alpha 3$	0,3	0,3	0,3	0,3

Table 2: C series

<b>Name</b>	C1	C2	C3	C4	C5	C6
Size PFDTs ( $\mu\text{m}$ )	2000	2000	2000	2000	2000	2000
Size S-P1 ( $\mu\text{m}$ )	<b>500</b>	<b>750</b>	<b>1250</b>	<b>1500</b>	<b>1750</b>	<b>2000</b>
$W_{SiO_2}$ ( $\mu\text{m}$ )	16	16	16	16	16	16
$W_{PFDTs}$ ( $\mu\text{m}$ )	14,4	14,4	14,4	14,4	14,4	14,4
$\alpha 1$	0,9	0,9	0,9	0,9	0,9	0,9
Size S-P2 ( $\mu\text{m}$ )	<b>500</b>	<b>750</b>	<b>1250</b>	<b>1500</b>	<b>1750</b>	<b>2000</b>
$W_{SiO_2}$ ( $\mu\text{m}$ )	16	16	16	16	16	16
$W_{PFDTs}$ ( $\mu\text{m}$ )	8	8	8	8	8	8
$\alpha 2$	0,5	0,5	0,5	0,5	0,5	0,5
Size S-P3 ( $\mu\text{m}$ )	<b>500</b>	<b>750</b>	<b>1250</b>	<b>1500</b>	<b>1750</b>	<b>2000</b>
$W_{SiO_2}$ ( $\mu\text{m}$ )	16	16	16	16	16	16
$W_{PFDTs}$ ( $\mu\text{m}$ )	4,8	4,8	4,8	4,8	4,8	4,8
$\alpha 3$	0,3	0,3	0,3	0,3	0,3	0,3

Table 3: D series

Name	D1	D2	D3	D4	D5	D6
Size PFDTS ( $\mu\text{m}$ )	2000	2000	2000	2000	2000	2000
Size S-P1 ( $\mu\text{m}$ )	1000	1000	1000	1000	1000	1000
$W_{SiO_2}$ ( $\mu\text{m}$ )	16	16	16	16	16	16
$W_{PFDTS}$ ( $\mu\text{m}$ )	14,4	14,4	14,4	14,4	14,4	14,4
$\alpha_1$	0,9	0,9	0,9	0,9	0,9	0,9
Size S-P2 ( $\mu\text{m}$ )	1000	1000	1000	1000	1000	1000
$W_{SiO_2}$ ( $\mu\text{m}$ )	16	16	16	16	16	16
$W_{PFDTS}$ ( $\mu\text{m}$ )	8	8	8	8	8	8
$\alpha_2$	0,5	0,5	0,5	0,5	0,5	0,5
Size S-P3 ( $\mu\text{m}$ )	1000	1000	1000	1000	1000	1000
$W_{SiO_2}$ ( $\mu\text{m}$ )	16	16	16	16	16	16
$W_{PFDTS}$ ( $\mu\text{m}$ )	7	6	5	4	3	2
$\alpha_3$	<b>0,4375</b>	<b>0,375</b>	<b>0,3125</b>	<b>0,25</b>	<b>0,1875</b>	<b>0,125</b>

Table 4: E series

Name	E1	E2	E3	E4	E5	E6	E7	E8
Size PFDTS ( $\mu\text{m}$ )	1500	1500	1500	1500	1500	1500	1500	1500
Size S-P1 ( $\mu\text{m}$ )	700	700	700	700	700	700	700	700
$W_{SiO_2}$ ( $\mu\text{m}$ )	<b>30</b>	<b>25</b>	<b>20</b>	<b>18</b>	<b>16</b>	<b>15</b>	<b>12</b>	<b>10</b>
$W_{PFDTS}$ ( $\mu\text{m}$ )	27	22,5	18	16,2	14,4	13,5	10,8	9
$\alpha_1$	0,9	0,9	0,9	0,9	0,9	0,9	0,9	0,9
Size S-P2 ( $\mu\text{m}$ )	700	700	700	700	700	700	700	700
$W_{SiO_2}$ ( $\mu\text{m}$ )	<b>30</b>	<b>25</b>	<b>20</b>	<b>18</b>	<b>16</b>	<b>15</b>	<b>12</b>	<b>10</b>
$W_{PFDTS}$ ( $\mu\text{m}$ )	15	12,5	10	9	8	7,5	6	5
$\alpha_2$	0,5	0,5	0,5	0,5	0,5	0,5	0,5	0,5
Size S-P3 ( $\mu\text{m}$ )	700	700	700	700	700	700	700	700
$W_{SiO_2}$ ( $\mu\text{m}$ )	<b>30</b>	<b>25</b>	<b>20</b>	<b>18</b>	<b>16</b>	<b>15</b>	<b>12</b>	<b>10</b>
$W_{PFDTS}$ ( $\mu\text{m}$ )	9	7,5	6	5,4	4,8	4,5	3,6	3
$\alpha_3$	0,3	0,3	0,3	0,3	0,3	0,3	0,3	0,3

Table 5: F series

Name	F1	F2	F3	F4	F5	F6	F7	F8
Size PFDTS ( $\mu\text{m}$ )	2000	2000	2000	2000	2000	2000	2000	2000
Size S-P1 ( $\mu\text{m}$ )	1000	1000	1000	1000	1000	1000	1000	1000
$W_{SiO_2}$ ( $\mu\text{m}$ )	<b>30</b>	<b>25</b>	<b>20</b>	<b>18</b>	<b>16</b>	<b>15</b>	<b>12</b>	<b>10</b>
$W_{PFDTS}$ ( $\mu\text{m}$ )	27	22,5	18	16,2	14,4	13,5	10,8	9
$\alpha 1$	0,9	0,9	0,9	0,9	0,9	0,9	0,9	0,9
Size S-P2 ( $\mu\text{m}$ )	1000	1000	1000	1000	1000	1000	1000	1000
$W_{SiO_2}$ ( $\mu\text{m}$ )	<b>30</b>	<b>25</b>	<b>20</b>	<b>18</b>	<b>16</b>	<b>15</b>	<b>12</b>	<b>10</b>
$W_{PFDTS}$ ( $\mu\text{m}$ )	15	12,5	10	9	8	7,5	6	5
$\alpha 2$	0,5	0,5	0,5	0,5	0,5	0,5	0,5	0,5
Size S-P3 ( $\mu\text{m}$ )	1000	1000	1000	1000	1000	1000	1000	1000
$W_{SiO_2}$ ( $\mu\text{m}$ )	<b>30</b>	<b>25</b>	<b>20</b>	<b>18</b>	<b>16</b>	<b>15</b>	<b>12</b>	<b>10</b>
$W_{PFDTS}$ ( $\mu\text{m}$ )	9	7,5	6	5,4	4,8	4,5	3,6	3
$\alpha 3$	0,3	0,3	0,3	0,3	0,3	0,3	0,3	0,3

Table 6: G series

Name	G1	G2	G3	G4	G5	G6	G7	G8
Size PFDTS ( $\mu\text{m}$ )	2000	2000	2000	2000	2000	2000	2000	2000
Size S-P1 ( $\mu\text{m}$ )	1000	1000	1000	1000	1000	1000	1000	1000
$W_{SiO_2}$ ( $\mu\text{m}$ )	16	16	16	16	16	16	16	16
$W_{PFDTS}$ ( $\mu\text{m}$ )	16	14,4	12,8	11,2	10,4	9,6	8,8	6,4
$\alpha 1$	<b>1</b>	<b>0,9</b>	<b>0,8</b>	<b>0,7</b>	<b>0,65</b>	<b>0,6</b>	<b>0,55</b>	<b>0,4</b>
Size S-P2 ( $\mu\text{m}$ )	1000	1000	1000	1000	1000	1000	1000	1000
$W_{SiO_2}$ ( $\mu\text{m}$ )	16	16	16	16	16	16	16	16
$W_{PFDTS}$ ( $\mu\text{m}$ )	4	4	4	4	4	4	4	4
$\alpha 2$	0,25	0,25	0,25	0,25	0,25	0,25	0,25	0,25
Size S-P3 ( $\mu\text{m}$ )	0	0	0	0	0	0	0	0
$W_{SiO_2}$ ( $\mu\text{m}$ )	0	0	0	0	0	0	0	0
$W_{PFDTS}$ ( $\mu\text{m}$ )	0	0	0	0	0	0	0	0
$\alpha 3$	0	0	0	0	0	0	0	0